particle pulse is short enough, the duration of the moderated neutron pulses is roughly inversely proportional to the neutron speed.

These accelerator-driven pulsed sources are pulsed at frequencies of between 10 and 100 Hz.

There are two fundamental differences between a reactor and a pulsed source.

(1) *All* experiments at a pulsed source must be performed with time-of-flight techniques. The pulsed source produces neutrons in bursts of 1 to 50 μs duration, depending on the energy, spaced about 10 to 100 ms apart, so that the duty cycle is low but there is very high neutron intensity within each pulse. The time-of-flight technique makes it possible to exploit that high intensity. With the de Broglie relationship, for neutrons

$$\lambda\,(\text{Å}) = 0.3966\,t\,(\mu s)/L\,(\text{cm}),$$

where t is the flight time in μs and L is the total flight path in cm.

(2) The spectral characteristics of pulsed sources are somewhat different from reactors in that they have a much larger component of higher-energy (above 100 meV) neutrons than the thermal spectrum at reactors. The exploitation of this new energy regime accompanied by the short pulse duration is one of the great opportunities presented by spallation sources.

Fig. 4.4.1.2 illustrates the essential difference between experiments at a steady-state source (left panel) and a pulsed source (right panel). We confine the discussion here to diffraction. If the time over which useful information is gathered is equivalent to the full period of the source Δt (the case suggested by the lower-right figure), the *peak flux* of the pulsed source is the effective parameter to compare with the flux of the steady-state source. Often this is not the case, so one makes a comparison in terms of *time-averaged flux* (centre panel). For the pulsed source, this is lowered from the peak flux by the duty cycle, but with the time-of-flight method one uses a large interval of the spectrum (shaded area). For the steady-state source, the time-averaged flux is high, but only a small wavelength slice (stippled area) is used in the experiment. It is the *integrals* of the two areas which must be compared; for the pulsed sources now being designed, the integral is generally favourable compared with present-day reactors. Finally, one can see from the central panel that high-energy neutrons (100–1000 meV) are especially plentiful at the pulsed sources. These various features can be exploited in the design of different kinds of experiments at pulsed sources.

4.4.2. Beam-definition devices (By I. S. Anderson and O. Schärpf)

4.4.2.1. *Introduction*

Neutron scattering, when compared with X-ray scattering techniques developed on modern synchrotron sources, is flux limited, but the method remains unique in the resolution and range of energy and momentum space that can be covered. Furthermore, the neutron magnetic moment allows details of microscopic magnetism to be examined, and polarized neutrons can be exploited through their interaction with both nuclear and electron spins.

Owing to the low primary flux of neutrons, the beam definition devices that play the role of defining the beam conditions (direction, divergence, energy, polarization, *etc.*) have to be highly efficient. Progress in the development of such devices not only results in higher-intensity beams but also allows new techniques to be implemented.

The following sections give a (non-exhaustive) review of commonly used beam-definition devices. The reader should keep in mind the fact that neutron scattering experiments are typically carried out with large beams (1 to 50 cm^2) and divergences between 5 and 30 mrad.

4.4.2.2. *Collimators*

A collimator is perhaps the simplest neutron optical device and is used to define the direction and divergence of a neutron beam. The most rudimentary collimator consists of two slits or pinholes

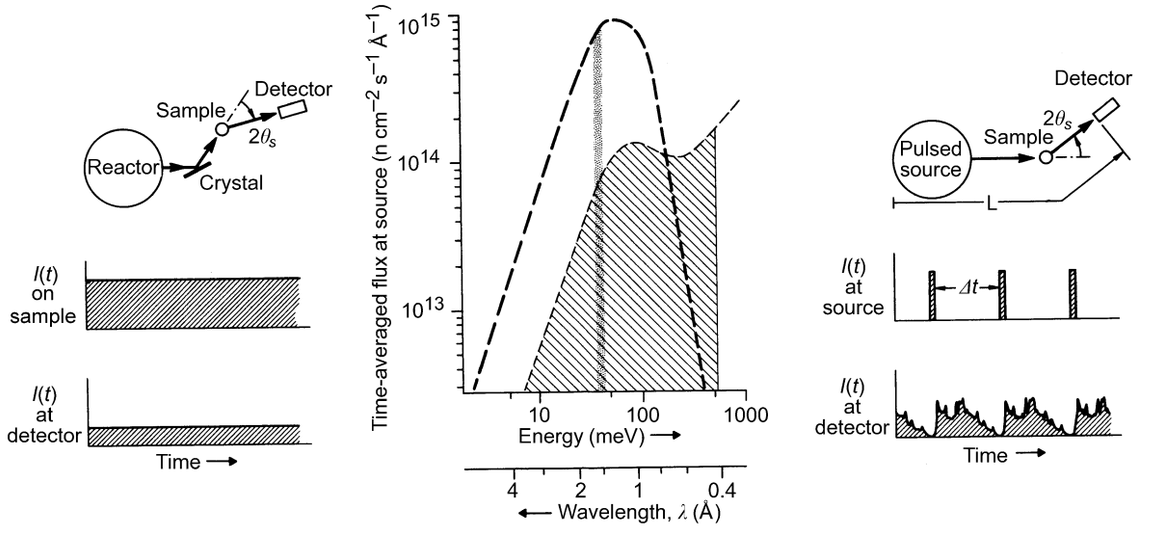

Fig. 4.4.1.2. Schematic diagram for performing diffraction experiments at steady-state and pulsed neutron sources. On the left we see the familiar monochromator crystal allowing a constant (in time) beam to fall on the sample (centre left), which then diffracts the beam through an angle $2\theta_s$ into the detector. The signal in the latter is also constant in time (lower left). On the right, the pulsed source allows a wide spectrum of neutrons to fall on the sample in sharp pulses separated by Δt (centre right). The neutrons are then diffracted by the sample through $2\theta_s$ and their time of arrival in the detector is analysed (lower right). The centre figure shows the time-averaged flux at the source. At a reactor, we make use of a narrow band of neutrons (heavy shading), here chosen with $\lambda = 1.5$ Å. At a pulsed source, we use a wide spectral band, here chosen from 0.4 to 3 Å and each one is identified by its time-of-flight. For the experimentalist, an important parameter is the integrated area of the two-shaded areas. Here they have been made identical.

cut into an absorbing material and placed one at the beginning and one at the end of a collimating distance L. The maximum beam divergence that is transmitted with this configuration is

$$\alpha_{\max} = (a_1 + a_2)/L, \qquad (4.4.2.1)$$

where a_1 and a_2 are the widths of the slits or pinholes.

Such a device is normally used for small-angle scattering and reflectometry. In order to avoid parasitic scattering by reflection from slit edges, very thin sheets of a highly absorbing material, *e.g.* gadolinium foils, are used as the slit material. Sometimes wedge-formed cadmium plates are sufficient. In cases where a very precise edge is required, cleaved single-crystalline absorbers such as gallium gadolinium garnet (GGG) can be employed.

To avoid high intensity losses when the distances are large, sections of neutron guide can be introduced between the collimators, as in, for example, small-angle scattering instruments with variable collimation. In this case, for maximum intensity at a given resolution (divergence), the collimator length should be equal to the camera length, *i.e.* the sample–detector distance (Schmatz, Springer, Schelten & Ibel, 1974).

As can be seen from (4.4.2.1), the beam divergence from a simple slit or pinhole collimator depends on the aperture size. In order to collimate (in one dimension) a beam of large cross section within a reasonable distance L, Soller collimators, composed of a number of equidistant neutron absorbing blades, are used. To avoid losses, the blades must be as thin and as flat as possible. If their surfaces do not reflect neutrons, which can be achieved by using blades with rough surfaces or materials with a negative scattering length, such as foils of hydrogen-containing polymers (Mylar is commonly used) or paper coated with neutron-absorbing paint containing boron or gadolinium (Meister & Weckerman, 1973; Carlile, Hey & Mack, 1977), the angular dependence of the transmission function is close to the ideal triangular form, and transmissions of 96% of the theoretical value can be obtained with 10′ collimation. If the blades of the Soller collimator are coated with a material whose critical angle of reflection is equal to $\alpha_{\max}/2$ (for one particular wavelength), then a square angular transmission function is obtained instead of the normal triangular function, thus doubling the theoretical transmission (Meardon & Wroe, 1977).

Soller collimators are often used in combination with single-crystal monochromators to define the wavelength resolution of an instrument but the Soller geometry is only useful for one-dimensional collimation. For small-angle scattering applications, where two-dimensional collimation is required, a converging 'pepper pot' collimator can be used (Nunes, 1974; Glinka, Rowe & LaRock, 1986).

Cylindrical collimators with radial blades are sometimes used to reduce background scattering from the sample environment. This type of collimator is particularly useful with position-sensitive detectors and may be oscillated about the cylinder axis to reduce the shadowing effect of the blades (Wright, Berneron & Heathman, 1981).

4.4.2.3. *Crystal monochromators*

Bragg reflection from crystals is the most widely used method for selecting a well defined wavelength band from a white neutron beam. In order to obtain reasonable reflected intensities and to match the typical neutron beam divergences, crystals that reflect over an angular range of 0.2 to 0.5° are typically employed. Traditionally, mosaic crystals have been used in preference to perfect crystals, although reflection from a mosaic crystal gives rise to an increase in beam divergence with a concomitant broadening of the selected wavelength band. Thus, collimators are often used together with mosaic monochromators to define the initial and final divergences and therefore the wavelength spread.

Because of the beam broadening produced by mosaic crystals, it was soon recognised that elastically deformed perfect crystals and crystals with gradients in lattice spacings would be more suitable candidates for focusing applications since the deformation can be modified to optimize focusing for different experimental conditions (Maier-Leibnitz, 1969).

Perfect crystals are used commonly in high-energy-resolution backscattering instruments, interferometry and Bonse–Hart cameras for ultra-small-angle scattering (Bonse & Hart, 1965).

An ideal mosaic crystal is assumed to comprise an agglomerate of independently scattering domains or mosaic blocks that are more or less perfect, but small enough that primary extinction does not come into play, and the intensity reflected by each block may be calculated using the kinematic theory (Zachariasen, 1945; Sears, 1997). The orientation of the mosaic blocks is distributed inside a finite angle, called the mosaic spread, following a distribution that is normally assumed to be Gaussian. The ideal neutron mosaic monochromator is not an ideal mosaic crystal but rather a mosaic crystal that is sufficiently thick to obtain a high reflectivity. As the crystal thickness increases, however, secondary extinction becomes important and must be accounted for in the calculation of the reflectivity. The model normally used is that developed by Bacon & Lowde (1948), which takes into account strong secondary extinction and a correction factor for primary extinction (Freund, 1985). In this case, the mosaic spread (usually defined by neutron scatterers as the full width at half maximum of the reflectivity curve) is not an intrinsic crystal property, but increases with wavelength and crystal thickness and can become quite appreciable at longer wavelengths.

Ideal monochromator materials should have a large scattering-length density, low absorption, incoherent and inelastic cross sections, and should be available as large single crystals with a suitable defect concentration. Relevant parameters for some typical neutron monochromator crystals are given in Table 4.4.2.1.

In principle, higher reflectivities can be obtained in neutron monochromators that are designed to operate in reflection geometry, but, because reflection crystals must be very large when takeoff angles are small, transmission geometry may be used. In that case, the optimization of crystal thickness can only be achieved for a small wavelength range.

Nickel has the highest scattering-length density, but, since natural nickel comprises several isotopes, the incoherent cross section is quite high. Thus, isotopic ^{58}Ni crystals have been grown as neutron monochromators despite their expense. Beryllium, owing to its large scattering-length density and low incoherent and absorption cross sections, is also an excellent candidate for neutron monochromators, but the mosaic structure of beryllium is difficult to modify, and the availability of good-quality single crystals is limited (Mücklich & Petzow, 1993). These limitations may be overcome in the near future, however, by building composite monochromators from thin beryllium blades that have been plastically deformed (May, Klimanek & Magerl, 1995).

Pyrolytic graphite is a highly efficient neutron monochromator if only a medium resolution is required (the minimum mosaic spread is of the order of 0.4°), owing to high reflectivities, which may exceed 90% (Shapiro & Chesser, 1972), but its use is limited to wavelengths above 1.5Å, owing to the rather large d spacing of the 002 reflection. Whenever better resolution at

Table 4.4.2.1. *Some important properties of materials used for neutron monochromator crystals (in order of increasing unit-cell volume)*

Material	Structure	Lattice constant(s) at 300 K a, c (Å)	Unit-cell volume $V_0(10^{-24}$ cm$^3)$	Coherent scattering length b (10^{-12} cm)	Square of scattering-length density 10^{-21} cm^{-4}	Ratio of incoherent to total scattering cross section $\sigma_{\rm inc}/\sigma_s$	Absorption cross section $\sigma_{\rm abs}$ (barns)* (at $\lambda = 1.8$ Å)	Atomic mass A	Debye temperature θ_D (K)	$A\theta_D^2$ (10^6 K^2)
Beryllium	h.c.p	a : 2.2856 c : 3.5832	16.2	0.779 (1)	9.25	6.5×10^{-4}	0.0076 (8)	9.013	1188	12.7
Iron	b.c.c.	a : 2.8664	23.5	0.954 (6)	6.59	0.033	2.56 (3)	55.85	411	9.4
Zinc	h.c.p.	a : 2.6649 c : 4.9468	30.4	0.5680 (5)	1.50	0.019	1.11 (2)	65.38	253	4.2
Pyrolytic graphite	layer hexag.	a : 2.461 c : 6.708	35.2	0.66484 (13)	5.71	$< 2 \times 10^{-4}$	0.00350 (7)	12.01	800	7.7
Niobum	b.c.c.	3.3006	35.9	0.7054 (3)	1.54	4×10^{-4}	1.15 (5)	92.91	284	7.5
Nickel (^{58}Ni)	f.c.c.	3.5241	43.8	1.44 (1)	17.3	0	4.6 (3)	58.71	417	9.9
Copper	f.c.c.	3.6147	47.2	0.7718 (4)	4.28	0.065	3.78 (2)	63.54	307	6.0
Aluminium	f.c.c.	4.0495	66.4	0.3449 (5)	0.43	5.6×10^{-3}	0.231 (3)	26.98	402	4.4
Lead	f.c.c.	4.9502	121	0.94003 (14)	0.97	2.7×10^{-4}	0.171 (2)	207.21	87	1.6
Silicon	diamond	5.4309	160	0.41491 (10)	0.43	6.9×10^{-3}	0.171 (3)	28.09	543	8.3
Germanium	diamond	5.6575	181	0.81929 (7)	1.31	0.020	2.3 (2)	72.60	290	6.1

* 1 barn= 10^{-28} m^2.

shorter wavelengths is required, copper (220 and 200) or germanium (311 and 511) monochromators are frequently used. The advantage of copper is that the mosaic structure can be easily modified by plastic deformation at high temperature. As with most face-centred cubic crystals, it is the (111) slip planes that are functional in generating the dislocation density needed for the desired mosaic spread, and, depending on the required orientation, either isotropic or anisotropic mosaics can be produced (Freund, 1976). The latter is interesting for vertical focusing applications, where a narrow vertical mosaic is required regardless of the resolution conditions.

Although both germanium and silicon are attractive as monochromators, owing to the absence of second-order neutrons for odd-index reflections, it is difficult to produce a controlled uniform mosaic spread in bulk samples by plastic deformation at high temperature because of the difficulty in introducing a spatially homogenous microstructure in large single crystals (Freund, 1975). Recently this difficulty has been overcome by building up composite monochromators from a stack of thin wafers, as originally proposed by Maier-Leibnitz (1967; Frey, 1974).

In practice, an artificial mosaic monochromator can be built up in two ways. In the first approach, illustrated in Fig. 4.4.2.1(*a*), the monochromator comprises a stack of crystalline wafers, each of which has a mosaic spread close to the global value required for the entire stack. Each wafer in the stack must be plastically deformed (usually by alternated bending) to produce the correct mosaic spread. For certain crystal orientations, the plastic deformation may result in an anisotropic mosaic spread. This method has been developed in several laboratories to construct germanium monochromators (Vogt, Passell, Cheung & Axe, 1994; Schefer *et al.*, 1996).

In the second approach, shown in Fig. 4.4.2.1(*b*), the global reflectivity distribution is obtained from the contributions of several stacked thin crystalline wafers, each with a rather narrow mosaic spread compared with the composite value but slightly misoriented with respect to the other wafers in the stack. If the misorientation of each wafer can be correctly controlled, this technique has the major advantage of producing monochromators with a highly anisotropic mosaic structure. The shape of the reflectivity curve can be chosen at will (Gaussian, Lorentzian, rectangular), if required. Moreover, because the initial mosaicity required is small, it is not necessary to use mosaic wafers and therefore for each wafer to undergo a long and tedious plastic deformation process. Recently, this method has been applied successfully to construct copper monochromators (Hamelin, Anderson, Berneron, Escoffier, Foltyn & Hehn, 1997), in which individual copper wafers were cut in a cylindrical form and then slid across one another to produce the required mosaic spread in the scattering plane. This technique looks very promising for the production of anisotropic mosaic monochromators.

The reflection from a mosaic crystal is visualized in Fig. 4.4.2.2(*b*). An incident beam with small divergence is transformed into a broad exit beam. The range of **k** vectors, Δk, selected in this process depends on the mosaic spread, η, and the incoming and outgoing beam divergences, α_1 and α_2.

$$\Delta k/k = \Delta\tau/\tau + \alpha\cot\theta, \tag{4.4.2.2}$$

where τ is the magnitude of the crystal reciprocal-lattice vector ($\tau = 2\pi/d$) and α is given by

$$\alpha = \sqrt{\frac{\alpha_1^2\alpha_2^2 + \alpha_1^2\eta^2 + \alpha_2^2\eta^2}{\alpha_1^2 + \alpha_2^2 + 4\eta^2.}} \tag{4.4.2.3}$$

The resolution can therefore be defined by collimators, and the highest resolution is obtained in backscattering, where the wavevector spread depends only on the intrinsic $\Delta d/d$ of the crystal.

In some applications, the beam broadening produced by mosaic crystals can be detrimental to the instrument performance. An interesting alternative is a gradient crystal, *i.e.* a single crystal with a smooth variation of the interplanar lattice spacing along a defined crystallographic direction. As shown in Fig. 4.4.2.2(*c*), the diffracted phase-space element has a different shape from that obtained from a mosaic crystal. Gradients in d spacing can be produced in various ways,

including thermal gradients (Alefeld, 1972), vibrating crystals by piezoelectric excitation (Hock, Vogt, Kulda, Mursic, Fuess & Magerl, 1993), and mixed crystals with concentration gradients, *e.g.* Cu–Ge (Freund, Guinet, Maréschal, Rustichelli & Vanoni, 1972) and Si–Ge (Maier-Leibnitz & Rustichelli, 1968; Magerl, Liss, Doll, Madar & Steichele, 1994).

Both vertically and horizontally focusing assemblies of mosaic crystals are employed to make better use of the neutron flux when making measurements on small samples. Vertical focusing can lead to intensity gain factors of between two and five without affecting resolution (real-space focusing) (Riste, 1970; Currat, 1973). Horizontal focusing changes the k-space volume that is selected by the monochromator through the variation in Bragg angle across the monochromator surface (k-space focusing) (Scherm, Dolling, Ritter, Schedler, Teuchert & Wagner, 1977). The orientation of the diffracted k-space volume can be modified by variation of the horizontal curvature, so that the resolution of the monochromator may be optimized with respect to a particular sample or experiment without loss of illumination. Monochromatic focusing can be achieved. Furthermore, asymmetrically cut crystals may be used, allowing focusing effects in real space and k space to be decoupled (Scherm & Kruger, 1994).

Traditionally, focusing monochromators consist of rectangular crystal plates mounted on an assembly that allows the orientation of each crystal to be varied in a correlated manner (Bührer, 1994). More recently, elastically deformed perfect crystals (in particular silicon) have been exploited as focusing elements for monochromators and analysers (Magerl & Wagner, 1994).

Since thermal neutrons have velocities that are of the order of km s^{-1}, their wavelengths can be Doppler shifted by diffraction from moving crystals. The k-space representation of the diffraction from a crystal moving perpendicular to its lattice planes is shown in Fig. 4.4.2.3(*a*). This effect is most commonly used in backscattering instruments on steady-state sources to vary the energy of the incident beam. Crystal velocities of 9–10 m s^{-1} are practically achievable, corresponding to energy variations of the order of $\pm$ 60 μeV.

The Doppler shift is also important in determining the resolution of the rotating-crystal time-of-flight (TOF) spectrom-

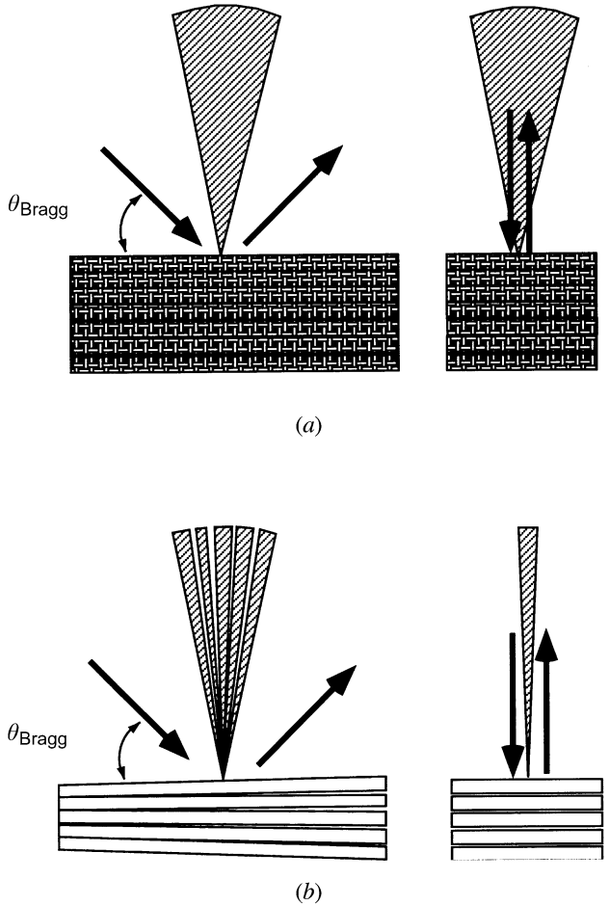

Fig. 4.4.2.1. Two methods by which artificial mosaic monochromators can be constructed: (*a*) out of a stack of crystalline wafers, each with a mosaicity close to the global value. The increase in divergence due to the mosaicity is the same in the horizontal (left picture) and the vertical (right picture) directions; (*b*) out of several stacked thin crystalline wafers each with a rather narrow mosaic but slightly misoriented in a perfectly controlled way. This allows the shape of the reflectivity curve to be rectangular, Gaussian, Lorentzian, *etc.*, and highly anisotropic, *i.e.* vertically narrow (right picture) and horizontally broad (left figure).

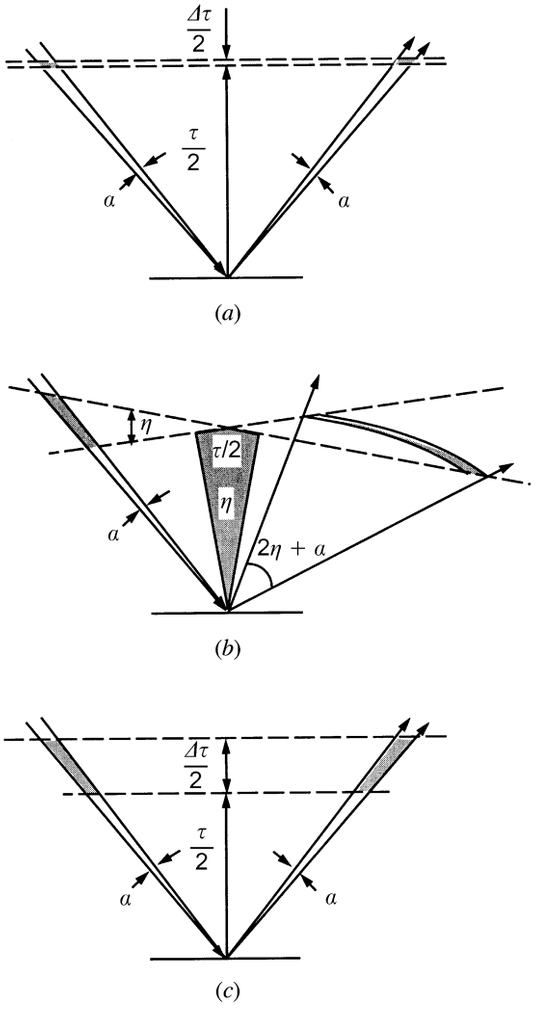

Fig. 4.4.2.2. Reciprocal-lattice representation of the effect of a monochromator with reciprocal-lattice vector τ on the reciprocal-space element of a beam with divergence α. (*a*) For an ideal crystal with a lattice constant width $\Delta\tau$; (*b*) for a mosaic crystal with mosaicity η, showing that a beam with small divergence, α, is transformed into a broad exit beam with divergence $2\eta + \alpha$; (*c*) for a gradient crystal with interplanar lattice spacing changing over $\Delta\tau$, showing that the divergence is not changed in this case.

eter, first conceived by Brockhouse (1958). A pulse of monochromatic neutrons is obtained when the reciprocal-lattice vector of a rotating crystal bisects the angle between two collimators. Effectively, the neutron **k** vector is changed in both direction and magnitude, depending on whether the crystal is moving towards or away from the neutron. For the rotating crystal, both of these situations occur simultaneously for different halves of the crystal, so that the net effect over the beam cross section is that a wider energy band is reflected than from the crystal at rest, and that, depending on the sense of rotation, the beam is either focused or defocused in time (Meister & Weckerman, 1972).

The Bragg reflection of neutrons from a crystal moving parallel to its lattice planes is illustrated in Fig. 4.4.2.3(*b*). It can be seen that the moving crystal selects a larger Δk than the crystal at rest, so that the reflected intensity is higher. Furthermore, it is possible under certain conditions to orientate the diffracted phase-space volume orthogonal to the diffraction vector. In this way, a monochromatic divergent beam can be obtained from a collimated beam with a larger energy spread. This provides an elegant means of producing a divergent beam with a sufficiently wide momentum spread to be scanned by the Doppler crystal of a backscattering instrument (Schelten & Alefeld, 1984).

Finally, an alternative method of scanning the energy of a monochromator in backscattering is to apply a steady but uniform temperature variation. The monochromator crystal must have a reasonable thermal expansion coefficient, and care has to be taken to ensure a uniform temperature across the crystal.

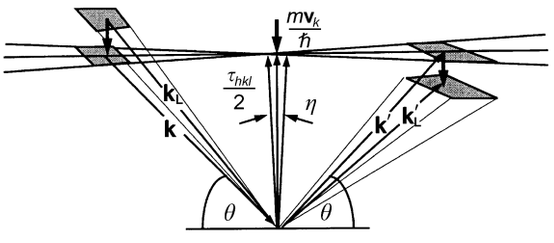

(*a*)

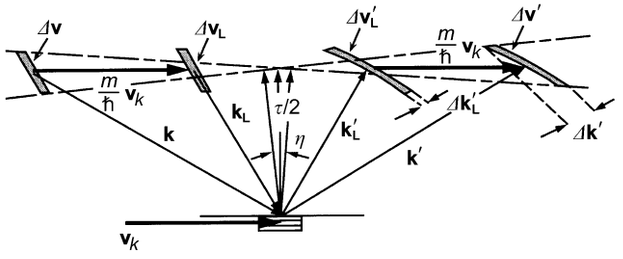

(*b*)

Fig. 4.4.2.3. Momentum-space representation of Bragg scattering from a crystal moving (*a*) perpendicular and (*b*) parallel to the diffracting planes with a velocity $\mathbf{v}_k$. The vectors $\mathbf{k}_L$ and $\mathbf{k}'_L$ refer to the incident and reflected wavevectors in the laboratory frame of reference. In (*a*), depending on the direction of $\mathbf{v}_k$, the reflected wavevector is larger or smaller than the incident wavevector, $\mathbf{k}_L$. In (*b*), a larger incident reciprocal-space volume, $\Delta\mathbf{v}_L$, is selected by the moving crystal than would have been selected by the crystal at rest. The reflected reciprocal-space element, $\Delta\mathbf{v}'_L$, has a large divergence, but can be arranged to be normal to $\mathbf{k}'_L$, hence improving the resolution $\Delta\mathbf{k}'_L$.

Table 4.4.2.2. *Neutron scattering-length densities, Nb_{coh}, for some commonly used materials*

Material	Nb (10^{-6} Å^{-2})
^{58}Ni	13.31
Diamond	11.71
Nickel	9.40
Quartz	3.64
Germanium	3.62
Silver	3.50
Aluminium	2.08
Silicon	2.08
Vanadium	−0.27
Titanium	−1.95
Manganese	−2.95

4.4.2.4. *Mirror reflection devices*

The refractive index, n, for neutrons of wavelength λ propagating in a nonmagnetic material of atomic density N is given by the expression

$$n^2 = 1 - \frac{\lambda^2 Nb_{\rm coh}}{\pi,} \qquad (4.4.2.4)$$

where $b_{\rm coh}$ is the mean coherent scattering length. Values of the scattering-length density $Nb_{\rm coh}$ for some common materials are listed in Table 4.4.2.2, from which it can be seen that the refractive index for most materials is slightly less than unity, so that total external reflection can take place. Thus, neutrons can be reflected from a smooth surface, but the critical angle of reflection, γ_c, given by

$$\gamma_c = \lambda \sqrt{\frac{Nb_{\rm coh}}{\pi}}, \qquad (4.4.2.5)$$

is small, so that reflection can only take place at grazing incidence. The critical angle for nickel, for example, is 0.1° Å^{-1}.

Because of the shallowness of the critical angle, reflective optics are traditionally bulky, and focusing devices tend to have long focal lengths. In some cases, however, depending on the beam divergence, a long mirror can be replaced by an equivalent stack of shorter mirrors.

4.4.2.4.1. *Neutron guides*

The principle of mirror reflection is the basis of neutron guides, which are used to transmit neutron beams to instruments that may be situated up to 100 m away from the source (Christ & Springer, 1962; Maier-Leibnitz & Springer, 1963). A standard neutron guide is constructed from boron glass plates assembled to form a rectangular tube, the dimensions of which may be up to 200 mm high by 50 mm wide. The inner surface of the guide is coated with approximately 1200 Å of either nickel, ^{58}Ni ($\gamma_c = 0.12^\circ$ Å^{-1}), or a 'supermirror' (described below). The guide is usually evacuated to reduce losses due to absorption and scattering of neutrons in air.

Theoretically, a neutron guide that is fully illuminated by the source will transmit a beam with a square divergence of full width $2\gamma_c$ in both the horizontal and vertical directions, so that the transmitted solid angle is proportional to λ^2. In practice, owing to imperfections in the assembly of the guide system, the divergence profile is closer to Gaussian than square at the end of a long guide. Since the neutrons may undergo a large number of reflections in the guide, it is important to achieve a high reflectivity. The specular reflectivity is determined by the surface roughness, and typically values in the range 98.5 to 99% are

achieved. Further transmission losses occur due to imperfections in the alignment of the sections that make up the guide.

The great advantage of neutron guides, in addition to the transport of neutrons to areas of low background, is that they can be multiplexed, *i.e.* one guide can serve many instruments. This is achieved either by deflecting only a part of the total cross section to a given instrument or by selecting a small wavelength range from the guide spectrum. In the latter case, the selection device (usually a crystal monochromator) must have a high transmission at other wavelengths.

If the neutron guide is curved, the transmission becomes wavelength dependent, as illustrated in Fig. 4.4.2.4. In this case, one can define a characteristic wavelength, λ^*, given by the relation $\theta^* = \sqrt{2a/\rho}$, so that

$$\lambda^* = \sqrt{\frac{\pi}{Nb_{\rm coh}}}\sqrt{\frac{2a}{\rho}} \qquad (4.4.2.6)$$

(where a is the guide width and ρ the radius of curvature), for which the theoretical transmission drops to 67%. For wavelengths less than λ^*, neutrons can only be transmitted by 'garland' reflections along the concave wall of the curved guide. Thus, the guide acts as a low-pass energy filter as long as its length is longer than the direct line-of-sight length $L_1 = \sqrt{8a\rho}$. For example, a 3 cm wide nickel-coated guide whose characteristic wavelength is 4 Å (radius of curvature 1300 m) must be at least 18 m long to act as a filter. The line-of-sight length can be reduced by subdividing the guide into a number of narrower channels, each of which acts as a miniguide. The resulting device, often referred to as a neutron bender, since deviation of the beam is achieved more rapidly, is used in beam deviators (Alefeld *et al.*, 1988) or polarizers (Hayter, Penfold & Williams, 1978). A microbender was devised by Marx (1971) in which the channels were made by evaporating alternate layers of aluminium (transmission layer) and nickel (mirror layer) onto a flexible smooth substrate.

Tapered guides can be used to reduce the beam size in one or two dimensions (Rossbach *et al.*, 1988), although, since mirror reflection obeys Liouville's theorem, focusing in real space is achieved at the expense of an increase in divergence. This fact can be used to calculate analytically the expected gain in neutron flux at the end of a tapered guide (Anderson, 1988). Alternatively, focusing can be achieved in one dimension using a bender in which the individual channel lengths are adjusted to create a focus (Freund & Forsyth, 1979).

4.4.2.4.2. *Focusing mirrors*

Optical imaging of neutrons can be achieved using ellipsoidal or torroidal mirrors, but, owing to the small critical angle of reflection, the dimensions of the mirrors themselves and the radii of curvature must be large. For example, a 4 m long toroidal mirror has been installed at the IN15 neutron spin echo spectrometer at the Institut Laue–Langevin, Grenoble (Hayes *et al.*, 1996), to focus neutrons with wavelengths greater than 15Å. The mirror has an in-plane radius of curvature of 408.75 m, and the sagittal radius is 280 mm. A coating of ^{65}Cu is used to obtain a high critical angle of reflection while maintaining a low surface roughness. Slope errors of less than 2.5×10^{-5} rad (r.m.s.) combined with a surface roughness of less than 3Å allow a minimum resolvable scattering vector of about 5×10^{-4} Å^{-1} to be reached.

For best results, the slope errors and the surface roughness must be low, in particular in small-angle scattering applications, since diffuse scattering from surface roughness gives rise to a halo around the image point. Owing to its low thermal expansion coefficient, highly polished Zerodur is often chosen as substrate.

4.4.2.4.3. *Multilayers*

Schoenborn, Caspar & Kammerer (1974) first pointed out that multibilayers, comprising alternating thin films of different scattering-length densities ($Nb_{\rm coh}$) act like two-dimensional crystals with a d spacing given by the bilayer period. With modern deposition techniques (usually sputtering), uniform films of thickness ranging from about twenty to a few hundred ångströms can be deposited over large surface areas of the order of 1 m^2. Owing to the rather large d spacings involved, the Bragg reflection from multilayers is generally at grazing incidence, so that long devices are required to cover a typical beam width, or a stacked device must be used. However, with judicious choice of the scattering-length contrast, the surface and interface roughness, and the number of layers, reflectivities close to 100% can be reached.

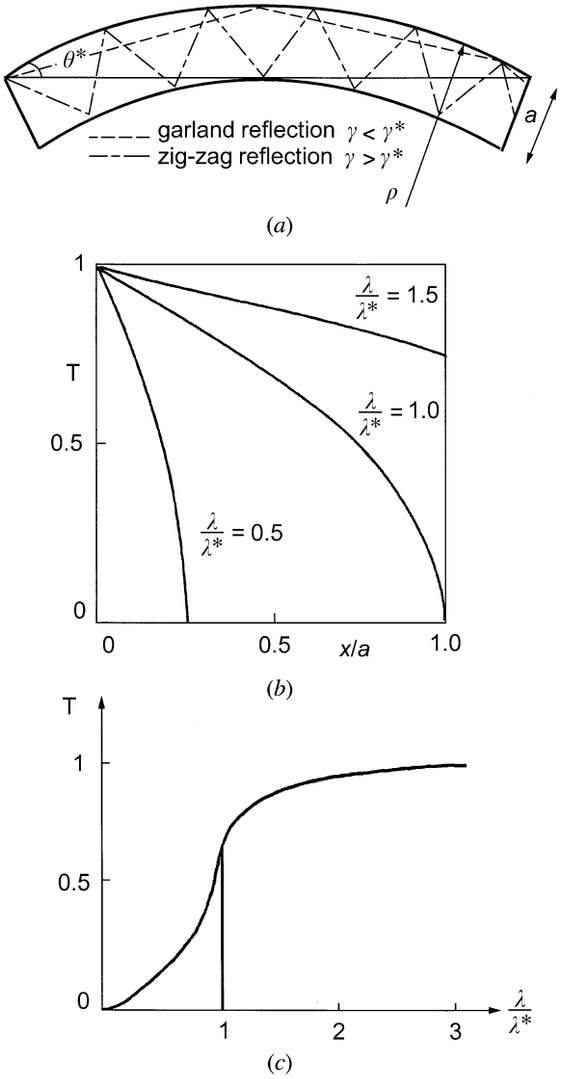

Fig. 4.4.2.4. In a curved neutron guide, the transmission becomes λ dependent: (*a*) the possible types of reflection (garland and zig-zag), the direct line-of-sight length, the critical angle θ^*, which is related to the characteristic wavelength $\lambda^* = \theta^*\sqrt{\pi/Nb_{\rm coh}}$; (*b*) transmission across the exit of the guide for different wavelengths, normalized to unity at the outside edge; (*c*) total transmission of the guide as a function of λ.

Fig. 4.4.2.5 illustrates how variation in the bilayer period can be used to produce a monochromator (the minimum $\Delta\lambda/\lambda$ that can be achieved is of the order of 0.5%), a broad-band device, or a 'supermirror', so called because it is composed of a particular sequence of bilayer thicknesses that in effect extends the region of total mirror reflection beyond the ordinary critical angle (Turchin, 1967; Mezei, 1976; Hayter & Mook, 1989). Supermirrors have been produced that extend the critical angle of nickel by a factor, m, of between three and four with reflectivities better than 90%. Such high reflectivities enable supermirror neutron guides to be constructed with flux gains, compared with nickel guides, close to the theoretical value of m^2.

The choice of the layer pairs depends on the application. For non-polarizing supermirrors and broad-band devices (Høghøj, Anderson, Ebisawa & Takeda, 1996), the Ni/Ti pair is commonly used, either pure or with some additions to relieve strain and stabilize interfaces (Elsenhans *et al.*, 1994) or alter the magnetism (Anderson & Høghøj, 1996), owing to the high contrast in scattering density, while for narrow-band monochromators a low contrast pair such as W/Si is more suitable.

4.4.2.4.4. *Capillary optics*

Capillary neutron optics, in which hollow glass capillaries act as waveguides, are also based on the concept of total external reflection of neutrons from a smooth surface. The advantage of capillaries, compared with neutron guides, is that the channel sizes are of the order of a few tens of micrometres, so that the radius of curvature can be significantly decreased for a given characteristic wavelength [see equation (4.4.2.6)]. Thus, neutrons can be efficiently deflected through large angles, and the device can be more compact.

Two basic types of capillary optics exist, and the choice depends on the beam characteristics required. Polycapillary fibres are manufactured from hollow glass tubes several centimetres in diameter, which are heated, fused and drawn multiple times until bundles of thousands of micrometre-sized channels are formed having an open area of up to 70% of the cross section. Fibre outer diameters range from 300 to 600 μm and contain hundreds or thousands of individual channels with inner diameters between 3 and 50 μm. The channel cross section is usually hexagonal, though square channels have been produced, and the inner channel wall surface roughness is typically less than 10 Å r.m.s., giving rise to very high reflectivities. The principal limitations on transmission efficiency are the open area, the acceptable divergence (note that the critical angle for glass is 1 mrad Å^{-1}) and reflection losses due to absorption and scattering. A typical optical device will comprise hundreds or thousands of fibres threaded through thin screens to produce the required shape.

Fig. 4.4.2.6 shows typical applications of polycapillary devices. In Fig. 4.4.2.6(*a*), a polycapillary lens is used to refocus neutrons collected from a divergent source. The half lens depicted in Fig. 4.4.2.6(*b*) can be used either to produce a nearly parallel (divergence $= 2\gamma_c$) beam from a divergent source or (in the reverse sense) to focus a nearly parallel beam, *e.g.* from a neutron guide. The size of the focal point depends on the channel size, the beam divergence, and the focal length of the lens. For example, a polycapillary lens used in a prompt γ-activation analysis instrument at the National Institute of Standards and Technology to focus a cold neutron beam from a neutron guide results in a current density gain of 80 averaged over the focused beam size of 0.53 mm (Chen *et al.*, 1995).

Fig. 4.4.2.6(*c*) shows another simple application of polycapillaries as a compact beam bender. In this case, such a bender may be more compact than an equivalent multichannel guide bender, although the accepted divergence will be less. Furthermore, as with curved neutron guides, owing to the wavelength dependence of the critical angle the capillary curvature can be used to filter out thermal or high-energy neutrons.

It should be emphasized that the applications depicted in Fig. 4.4.2.6 obey Liouville's theorem, in that the density of neutrons in phase space is not changed, but the shape of the phase-space volume is altered to meet the requirements of the experiment,

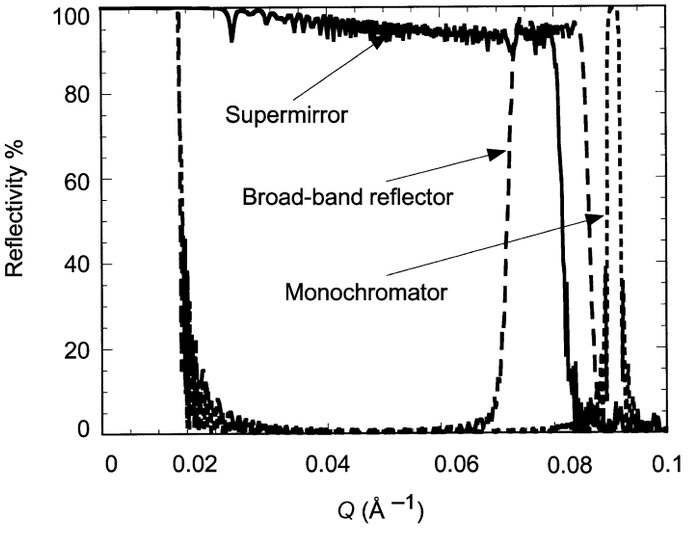

Fig. 4.4.2.5. Illustration of how a variation in the bilayer period can be used to produce a monochromator, a broad-band device, or a supermirror.

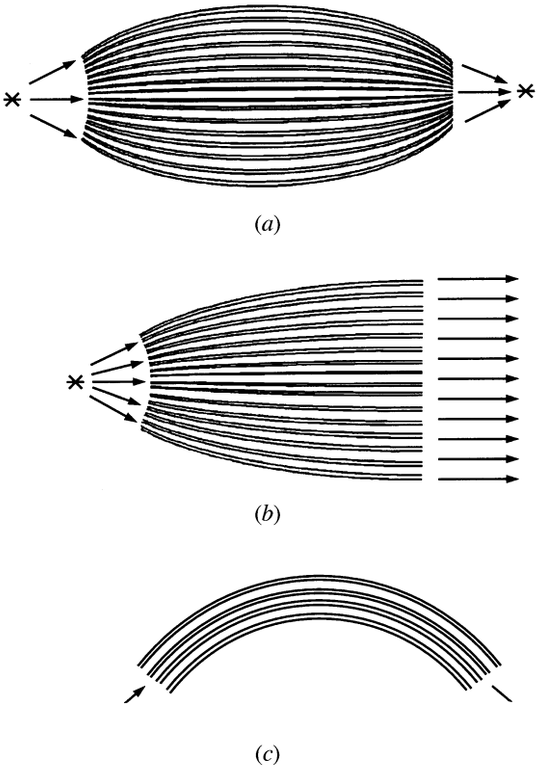

Fig. 4.4.2.6. Typical applications of polycapillary devices: (*a*) lens used to refocus a divergent beam; (*b*) half-lens to produce a nearly parallel beam or to focus a nearly parallel beam; (*c*) a compact bender.

i.e. there is a simple trade off between beam dimension and divergence.

The second type of capillary optic is a monolithic configuration. The individual capillaries in monolithic optics are tapered and fused together, so that no external frame assembly is necessary (Chen-Mayer *et al.*, 1996). Unlike the multifibre devices, the inner diameters of the channels that make up the monolithic optics vary along the length of the component, resulting in a smaller more compact design.

Further applications of capillary optics include small-angle scattering (Mildner, 1994) and lenses for high-spatial-resolution area detection.

4.4.2.5. *Filters*

Neutron filters are used to remove unwanted radiation from the beam while maintaining as high a transmission as possible for the neutrons of the required energy. Two major applications can be identified: removal of fast neutrons and γ-rays from the primary beam and reduction of higher-order contributions (λ/n) in the secondary beam reflected from crystal monochromators. In this section, we deal with non-polarizing filters, *i.e.* those whose transmission and removal cross sections are independent of the neutron spin. Polarizing filters are discussed in the section concerning polarizers.

Filters rely on a strong variation of the neutron cross section with energy, usually either the wavelength-dependent scattering cross section of polycrystals or a resonant absorption cross section. Following Freund (1983), the total cross section determining the attenuation of neutrons by a crystalline solid can be written as a sum of three terms,

$$\sigma = \sigma_{\rm abs} + \sigma_{\rm tds} + \sigma_{\rm Bragg}. \qquad (4.4.2.7)$$

Here, $\sigma_{\rm abs}$ is the true absorption cross section, which, at low energy, away from resonances, is proportional to $E^{-1/2}$. The temperature-dependent thermal diffuse cross section, $\sigma_{\rm tds}$, describing the attenuation due to inelastic processes, can be split into two parts depending on the neutron energy. At low energy, $E \ll k_b\Theta_D$, where k_b is Boltzmann's constant and Θ_D is the characteristic Debye temperature, single-phonon processes dominate, giving rise to a cross section, $\sigma_{\rm sph}$, which is also proportional to $E^{-1/2}$. The single-phonon cross section is proportional to $T^{7/2}$ at low temperatures and to T at higher temperatures. At higher energies, $E \geq k_b\Theta_D$, multiphonon and multiple-scattering processes come into play, leading to a cross section, $\sigma_{\rm mph}$, that increases with energy and temperature. The third contribution, $\sigma_{\rm Bragg}$, arises due to Bragg scattering in single- or polycrystalline material. At low energies, below the Bragg cut-off ($\lambda > 2d_{\rm max}$), $\sigma_{\rm Bragg}$ is zero. In polycrystalline materials, the cross section rises steeply above the Bragg cut-off and oscillates with increasing energy as more reflections come into play. At still higher energies, $\sigma_{\rm Bragg}$ decreases to zero.

In single-crystalline material above the Bragg cut-off, $\sigma_{\rm Bragg}$ is characterized by a discrete spectrum of peaks whose heights and widths depend on the beam collimation, energy resolution, and the perfection and orientation of the crystal. Hence a monocrystalline filter has to be tuned by careful orientation.

The resulting attenuation cross section for beryllium is shown in Fig. 4.4.2.7. Cooled polycrystalline beryllium is frequently used as a filter for neutrons with energies less than 5 meV, since there is an increase of nearly two orders of magnitude in the attenuation cross section for higher energies. BeO, with a Bragg cut-off at approximately 4 meV, is also commonly used.

Pyrolytic graphite, being a layered material with good crystalline properties along the c direction but random orientation perpendicular to it, lies somewhere between a polycrystal and a single crystal as far as its attenuation cross section is concerned. The energy-dependent cross section for a neutron beam incident along the c axis of a pyrolytic graphite filter is shown in Fig. 4.4.2.8, where the attenuation peaks due to the 00ξ reflections can be seen. Pyrolytic graphite serves as an efficient second- or third-order filter (Shapiro & Chesser, 1972) and can be 'tuned' by slight misorientation away from the c axis.

Further examples of typical filter materials (*e.g.* silicon, lead, bismuth, sapphire) can be found in the paper by Freund (1983).

Resonant absorption filters show a large increase in their attenuation cross sections at the resonant energy and are therefore used as selective filters for that energy. A list of typical filter materials and their resonance energies is given in Table 4.4.2.3.

4.4.2.6. *Polarizers*

Methods used to polarize a neutron beam are many and varied, and the choice of the best technique depends on the instrument and the experiment to be performed. The main parameter that has to be considered when describing the effectiveness of a given polarizer is the polarizing efficiency, defined as

$$P = (N_+ - N_-)/(N_+ + N_-), \qquad (4.4.2.8)$$

where N_+ and N_- are the numbers of neutrons with spin parallel (+) or antiparallel (−) to the guide field in the outgoing beam. The second important factor, the transmission of the wanted spin state, depends on various factors, such as acceptance angles, reflection, and absorption.

4.4.2.6.1. *Single-crystal polarizers*

The principle by which ferromagnetic single crystals are used to polarize and monochromate a neutron beam simultaneously is shown in Fig. 4.4.2.9. A field **B**, applied perpendicular to the scattering vector $\boldsymbol{\kappa}$, saturates the atomic moments $\mathbf{M}_\nu$ along the field direction. The cross section for Bragg reflection in this geometry is

$$(\mathrm{d}\sigma/\mathrm{d}\Omega) = F_N(\boldsymbol{\kappa})^2 + 2F_N(\boldsymbol{\kappa})F_M(\boldsymbol{\kappa})(\mathbf{P}\cdot\boldsymbol{\mu}) + F_M(\boldsymbol{\kappa})^2, \quad (4.4.2.9)$$

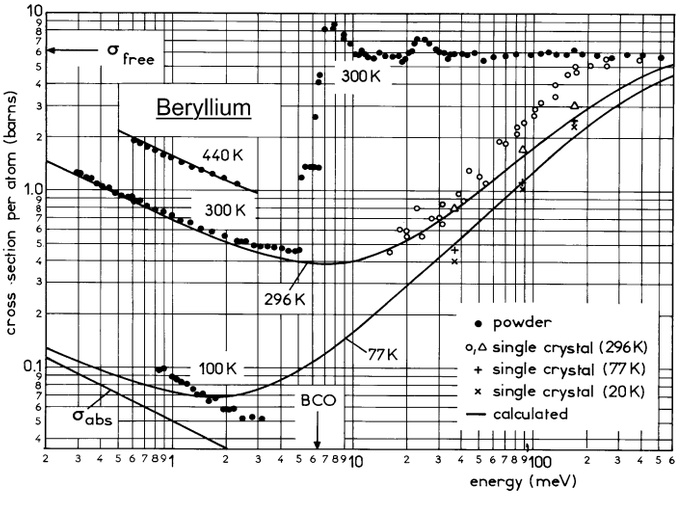

Fig. 4.4.2.7. Total cross section for beryllium in the energy range where it can be used as a filter for neutrons with energy below 5 meV (Freund, 1983).

Table 4.4.2.3. *Characteristics of some typical elements and isotopes used as neutron filters*

Element or isotope	Resonance (eV)	σ_s (resonance) (barns)	λ (Å)	$\sigma_s(\lambda)$ (barns)	$\frac{\sigma_s(\lambda/2)}{\sigma_s(\lambda)}$
In	1.45	30000	0.48	94	319
Rh	1.27	4500	0.51	76	59.2
Hf	1.10	5000	0.55	58	86.2
^{240}Pu	1.06	115000	9.55	145	793
Ir	0.66	4950	0.70	183	27.0
^{229}Th	0.61	6200	0.73	<100	>62.0
Er	0.58	1500	0.75	127	11.8
Er	0.46	2300	0.84	125	18.4
Eu	0.46	10100	0.84	1050	9.6
^{231}Pa	0.39	4900	0.92	116	42.2
^{239}Pu	0.29	5200	1.06	700	7.4

1 barn $= 10^{-28}$ m^2.

where $F_N(\boldsymbol{\kappa})$ is the nuclear structure factor and $F_M(\boldsymbol{\kappa}) = [(\gamma/2)r_0] \sum_\nu M_\nu f(hkl) \exp[2\pi(hx + ky + lz)]$ is the magnetic structure factor, with $f(hkl)$ the magnetic form factor of the magnetic atom at the position (x, y, z) in the unit cell. The vector $\mathbf{P}$ describes the polarization of the incoming neutron with respect to $\mathbf{B}$; $\mathbf{P} = 1$ for $+$ spins and $\mathbf{P} = -1$ for $-$ spins and $\boldsymbol{\mu}$ is a unit vector in the direction of the atomic magnetic moments. Hence, for neutrons polarized parallel to $\mathbf{B}$ $(\mathbf{P} \cdot \boldsymbol{\mu} = 1)$, the diffracted intensity is proportional to $[F_N(\boldsymbol{\kappa}) + F_M(\boldsymbol{\kappa})]^2$, while, for neutrons polarized antiparallel to $\mathbf{B}$ $(\mathbf{P} \cdot \boldsymbol{\mu} = -1)$, the diffracted intensity is proportional to $[F_N(\boldsymbol{\kappa}) - F_M(\boldsymbol{\kappa})]^2$. The polarizing efficiency of the diffracted beam is then

$$P = \pm 2F_N(\boldsymbol{\kappa})F_M(\boldsymbol{\kappa})/[F_N(\boldsymbol{\kappa})^2 + F_M(\boldsymbol{\kappa})^2], \qquad (4.4.2.10)$$

which can be either positive or negative and has a maximum value for $|F_N(\boldsymbol{\kappa})| = |F_M(\boldsymbol{\kappa})|$. Thus, a good single-crystal polarizer, in addition to possessing a crystallographic structure in which F_N and F_M are matched, must be ferromagnetic at room temperature and should contain atoms with large magnetic moments. Furthermore, large single crystals with 'controllable' mosaic should be available. Finally, the structure factor for the required reflection should be high, while those for higher-order reflections should be low.

None of the three naturally occurring ferromagnetic elements (iron, cobalt, nickel) makes efficient single-crystal polarizers. Cobalt is strongly absorbing and the nuclear scattering lengths of iron and nickel are too large to be balanced by their weak magnetic moments. An exception is ^{57}Fe, which has a rather low nuclear scattering length, and structure-factor matching can be achieved by mixing ^{57}Fe with Fe and 3% Si (Reed, Bolling & Harmon, 1973).

In general, in order to facilitate structure-factor matching, alloys rather than elements are used. The characteristics of some alloys used as polarizing monochromators are presented in Table 4.4.2.4. At short wavelengths, the 200 reflection of $Co_{0.92}Fe_{0.08}$ is used to give a positively polarized beam [$F_N(\boldsymbol{\kappa})$ and $F_M(\boldsymbol{\kappa})$ both positive], but the absorption due to cobalt is high. At longer wavelengths, the 111 reflection of the Heusler alloy Cu_2MnAl (Delapalme, Schweizer, Couderchon & Perrier de la Bathie, 1971; Freund, Pynn, Stirling & Zeyen, 1983) is commonly used, since it has a higher reflectivity and a larger d spacing than $Co_{0.92}Fe_{0.08}$. Since for the 111 reflection $F_N \approx -F_M$, the diffracted beam is negatively polarized. Unfortunately, the structure factor of the 222 reflection is higher than that of the 111 reflection, leading to significant higher-order contamination of the beam.

Other alloys that have been proposed as neutron polarizers are $Fe_{3-x}Mn_xSi$, $^7Li_{0.5}Fe_{2.5}O_4$ (Bednarski, Dobrzynski & Steinsvoll, 1980), Fe_3Si (Hines *et al.*, 1976), Fe_3Al (Pickart & Nathans, 1961), and $HoFe_2$ (Freund & Forsyth, 1979).

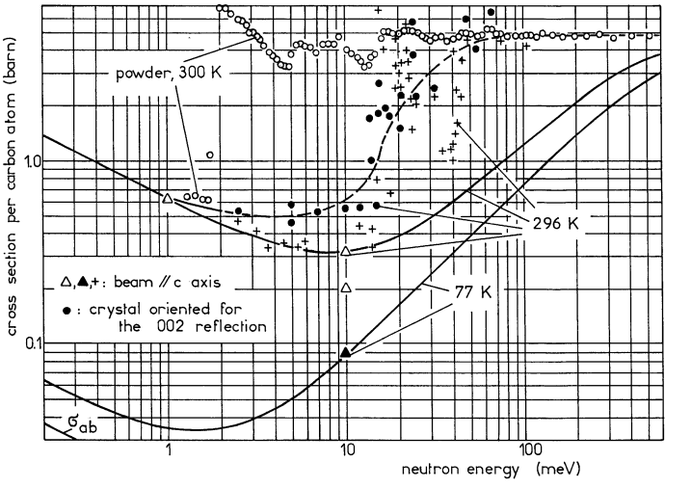

Fig. 4.4.2.8. Energy-dependent cross section for a neutron beam incident along the c axis of a pyrolytic graphite filter. The attenuation peaks due to the 00ξ reflections can be seen.

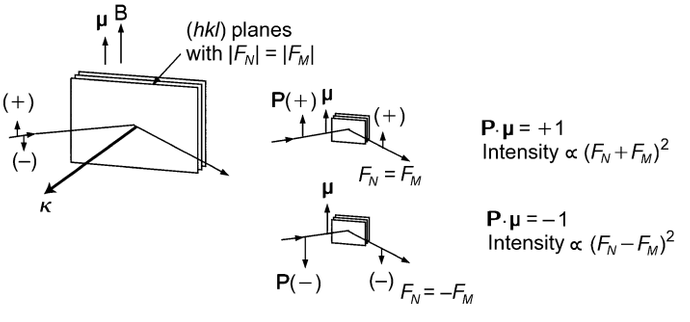

Fig. 4.4.2.9. Geometry of a polarizing monochromator showing the lattice planes (hkl) with $|F_N| = |F_M|$, the direction of $\mathbf{P}$ and $\boldsymbol{\mu}$, the expected spin direction and intensity.

Table 4.4.2.4. *Properties of polarizing crystal monochromators (Williams, 1988)*

	$Co_{0.92}Fe_{0.08}$	Cu_2MnAl	Fe_3Si	^{57}Fe:Fe	$HoFe_2$
Matched reflection $\|F_N\| \sim \|F_M\|$	200	111	111	110	620
d spacing (Å)	1.76	3.43	3.27	2.03	1.16
Take-off angle $2\theta_B$ at 1Å (°)	33.1	16.7	17.6	28.6	50.9
Cut-off wavelength, λ_{max} (Å)	3.5	6.9	6.5	4.1	2.3

4.4.2.6.2. *Polarizing mirrors*

For a ferromagnetic material, the neutron refractive index is given by

$$n_{\pm}^2 = 1 - \lambda^2 N(b_{coh} \pm p)/\pi, \qquad (4.4.2.11)$$

where the magnetic scattering length, p, is defined by

$$p = 2\mu(B - H)m\pi/h^2N. \qquad (4.4.2.12)$$

Here, m and μ are the neutron mass and magnetic moment, B is the magnetic induction in an applied field H, and h is Planck's constant.

The $-$ and $+$ signs refer, respectively, to neutrons whose moments are aligned parallel and antiparallel to B. The refractive index depends on the orientation of the neutron spin with respect to the film magnetization, thus giving rise to two critical angles of total reflection, γ_- and γ_+. Thus, reflection in an angular range between these two critical angles gives rise to polarized beams in reflection and in transmission. The polarization efficiency, P, is defined in terms of the reflectivity r_+ and r_- of the two spin states,

$$P = (r_+ - r_-)/(r_+ + r_-). \qquad (4.4.2.13)$$

The first polarizers using this principle were simple cobalt mirrors (Hughes & Burgy, 1950), while Schaerpf (1975) used FeCo sheets to build a polarizing guide. It is more common these days to use thin films of ferromagnetic material deposited onto a substrate of low surface roughness (*e.g.* float glass or polished silicon). In this case, the reflection from the substrate can be eliminated by including an antireflecting layer made from, for example, Gd–Ti alloys (Drabkin *et al.*, 1976). The major limitation of these polarizers is that grazing-incidence angles must be used and the angular range of polarization is small. This limitation can be partially overcome by using multilayers, as described above, in which one of the layer materials is ferromagnetic. In this case, the refractive index of the ferromagnetic material is matched for one spin state to that of the non-magnetic material, so that reflection does not occur. A polarizing supermirror made in this way has an extended angular range of polarization, as indicated in Fig. 4.4.2.10. It should be noted that modern deposition techniques allow the refractive index to be adjusted readily, so that matching is easily achieved. The scattering-length densities of some commonly used layer pairs are given in Table 4.4.2.5

Polarizing multilayers are also used in monochromators and broad-band devices. Depending on the application, various layer pairs have been used: Co/Ti, Fe/Ag, Fe/Si, Fe/Ge, Fe/W, FeCoV/TiN, FeCoV/TiZr, $^{63}Ni_{0.66}{}^{54}Fe_{0.34}$/V and the range of fields used to achieve saturation varies from about 100 to 500 Gs.

Polarizing mirrors can be used in reflection or transmission with polarization efficiencies reaching 97%, although, owing to the low incidence angles, their use is generally restricted to wavelengths above 2 Å.

Various devices have been constructed that use mirror polarizers, including simple reflecting mirrors, V-shaped transmission polarizers (Majkrzak, Nunez, Copley, Ankner & Greene, 1992), cavity polarizers (Mezei, 1988), and benders (Hayter, Penfold & Williams, 1978; Schaerpf, 1989). Perhaps the best known device is the polarizing bender developed by Schärpf. The device consists of 0.2 mm thick glass blades coated on both sides with a Co/Ti supermirror on top of an antireflecting Gd/Ti coating designed to reduce the scattering of the unwanted spin state from the substrate to a very low Q value. The device is quite compact (typically 30 cm long for a beam cross section up to 6×5 cm) and transmits over 40% of an unpolarized beam with the collimation from a nickel-coated guide for wavelengths above 4.5 Å. Polarization efficiencies of over 96% can be achieved with these benders.

4.4.2.6.3. *Polarizing filters*

Polarizing filters operate by selectively removing one of the neutron spin states from an incident beam, allowing the other spin state to be transmitted with only moderate attenuation. The spin selection is obtained by preferential absorption or scattering, so the polarizing efficiency usually increases with the thickness of the filter, whereas the transmission decreases. A compromise must therefore be made between polarization, P, and transmission, T. The 'quality factor' often used is $P\sqrt{T}$ (Tasset & Resouche, 1995).

The total cross sections for a generalized filter may be written as

$$\sigma_{\pm} = \sigma_0 \pm \sigma_p, \qquad (4.4.2.14)$$

where σ_0 is a spin-independent cross section and $\sigma_p = (\sigma_+ + \sigma_-)/2$ is the polarization cross section. It can be

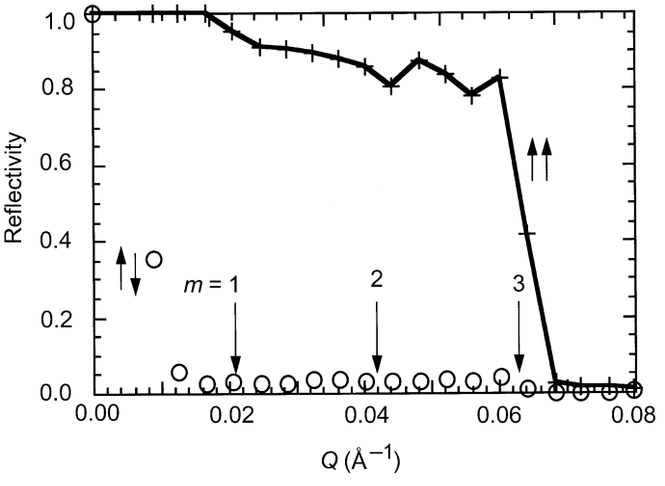

Fig. 4.4.2.10. Measured reflectivity curve of an FeCoV/TiZr polarizing supermirror with an extended angular range of polarization of three times that of γ_c(Ni) for neutrons without spin flip, ↑↑, and with spin flip, ↑↓.

Table 4.4.2.5. *Scattering-length densities for some typical materials used for polarizing multilayers*

Magnetic layer	$N(b+p)$ (10^{-6} Å^{-2})	$N(b-p)$ (10^{-6} Å^{-2})	Nb (10^{-6} Å^{-2})	Nonmagnetic layer
Fe	13.04	3.08	3.64	Ge
			3.50	Ag
			3.02	W
			2.08	Si
			2.08	Al
Fe:Co (50:50)	10.98	−0.52	−0.27	V
			−1.95	Ti
Ni	10.86	7.94		
Fe:Co:V (49:49:2)	10.75	−0.63	−0.27	V
			−1.95	Ti
Fe:Co:V (50:48:2)	10.66	−0.64	−0.27	V
			−1.95	Ti
Fe:Ni (50:50)	10.53	6.65		
Co	6.65	−2.00	−1.95	Ti
Fe:Co:V (52:38:10)	6.27	2.12	2.08	Si
			2.08	Al

For the non-magnetic layer we have only listed the simple elements that give a close match to the $N(b-p)$ value of the corresponding magnetic layer. In practice excellent matching can be achieved by using alloys (*e.g.* Ti_xZr_y alloys allow Nb values between −1.95 and 3.03×10^{-6}Å^{-2} to be selected) or reactive sputtering (*e.g.*TiN_x).

shown (Williams, 1988) that the ratio σ_p/σ_0 must be ≥ 0.65 to achieve $|P| > 0.95$ and $T > 0.2$.

Magnetized iron was the first polarizing filter to be used (Alvarez & Bloch, 1940). The method relies on the spin-dependent Bragg scattering from a magnetized polycrystalline block, for which σ_p approaches 10 barns near the Fe cut-off at 4 Å (Steinberger & Wick, 1949). Thus, for wavelengths in the range 3.6 to 4 Å, the ratio $\sigma_p/\sigma_0 \simeq 0.59$, resulting in a theoretical polarizing efficiency of 0.8 for a transmittance of ~ 0.3. In practice, however, since iron cannot be fully saturated, depolarization occurs, and values of $P \simeq 0.5$ with $T \sim 0.25$ are more typical.

Resonance absorption polarization filters rely on the spin dependence of the absorption cross section of polarized nuclei at their nuclear resonance energy and can produce efficient polarization over a wide energy range. The nuclear polarization is normally achieved by cooling in a magnetic field, and filters based on ^{149}Sm ($E_r = 0.097$ eV) (Freeman & Williams, 1978) and ^{151}Eu ($E_r = 0.32$ and 0.46 eV) have been successfully tested. The ^{149}Sm filter has a polarizing efficiency close to 1 within a small wavelength range (0.85 to 1.1 Å), while the transmittance is about 0.15. Furthermore, since the filter must be operated at temperatures of the order of 15 mK, it is very sensitive to heating by γ-rays.

Broad-band polarizing filters, based on spin-dependent scattering or absorption, provide an interesting alternative to polarizing mirrors or monochromators, owing to the wider range of energy and scattering angle that can be accepted. The most promising such filter is polarized ^{3}He, which operates through the huge spin-dependent neutron capture cross section that is totally dominated by the resonance capture of neutrons with antiparallel spin. The polarization efficiency of an ^{3}He neutron spin filter of length l can be written as

$$P_n(\lambda) = \tanh[\mathcal{O}(\lambda)P_{\rm He}], \qquad (4.4.2.15)$$

where $P_{\rm He}$ is the ^{3}He polarization, and $\mathcal{O}(\lambda) = [^3\mathrm{He}]l\sigma_0(\lambda)$ is the dimensionless effective absorption coefficient, also called the opacity (Surkau *et al.*, 1997). For gaseous ^{3}He, the opacity can be written in more convenient units as

$$\mathcal{O}' = p[\mathrm{bar}] \times l[\mathrm{cm}] \times \lambda[\text{Å}], \qquad (4.4.2.16)$$

where p is the ^{3}He pressure (1 bar = 10^5 Pa) and $\mathcal{O} = 7.33 \times 10^{-2}\mathcal{O}'$. Similarly, the residual transmission of the spin filter is given by

$$T_n(\lambda) = \exp[-\mathcal{O}(\lambda)]\cosh[\mathcal{O}(\lambda)P_{\rm He}]. \qquad (4.4.2.17)$$

It can be seen that, even at low ^{3}He polarization, full neutron polarization can be achieved in the limit of large absorption at the cost of the transmission.

^{3}He can be polarized either by spin exchange with optically pumped rubidium (Bouchiat, Carver & Varnum, 1960; Chupp, Coulter, Hwang, Smith & Welsh, 1996; Wagshul & Chupp, 1994) or by pumping of metastable ^{3}He* atoms followed by metastable exchange collisions (Colegrove, Schearer & Walters, 1963). In the former method, the ^{3}He gas is polarized at the required high pressure, whereas ^{3}He* pumping takes place at a pressure of about 1 mbar, followed by a polarization conserving compression by a factor of nearly 10 000. Although the polarization time constant for Rb pumping is of the order of several hours compared with fractions of a second for ^{3}He* pumping, the latter requires several 'fills' of the filter cell to achieve the required pressure.

An alternative broad-band spin filter is the polarized proton filter, which utilizes the spin dependence of nuclear scattering. The spin-dependent cross section can be written as (Lushchikov, Taran & Shapiro, 1969)

$$\sigma_\pm = \sigma_1 + \sigma_2 P_{\rm H}^2 \mp \sigma_3 P_{\rm H}, \qquad (4.4.2.18)$$

where σ_1, σ_2, and σ_3 are empirical constants. The viability of the method relies on achieving a high nuclear polarization $P_{\rm H}$. A polarization $P_{\rm H} = 0.7$ gives $\sigma_p/\sigma_0 \approx 0.56$ in the cold-neutron region. Proton polarizations of the order of 0.8 are required for a useful filter (Schaerpf & Stuesser, 1989). Polarized proton filters can polarize very high energy neutrons even in the eV range.

4.4.2.6.4. *Zeeman polarizer*

The reflection width of perfect silicon crystals for thermal neutrons and the Zeeman splitting ($\Delta E = 2\mu B$) of a field of about 10 kGs are comparable and therefore can be used to polarize a neutron beam. For a monochromatic beam (energy E_0) in a strong magnetic field region, the result of the Zeeman splitting will be a separation into two polarized subbeams, one polarized along **B** with energy $E_0 + \mu B$, and the other polarized antiparallel to **B** with energy $E_0 - \mu B$. The two polarized beams can be selected by rocking a perfect crystal in the field region B (Forte & Zeyen, 1989).

4.4.2.7. *Spin-orientation devices*

Polarization is the state of spin orientation of an assembly of particles in a target or beam. The beam polarization vector **P** is defined as the vector average of this spin state and is often described by the density matrix $\rho = \frac{1}{2}(1 + \sigma\mathbf{P})$. The polarization is then defined as $\mathbf{P} = \mathrm{Tr}(\rho\sigma)$. If the polarization vector is inclined to the field direction in a homogenous magnetic field, **B**, the polarization vector will precess with the classical Larmor frequency $\omega_L = |\gamma|B$. This results in a precessing spin polarization. For most experiments, it is sufficient to consider the linear polarization vector in the direction of an applied magnetic field. If, however, the magnetic field direction changes along the path of the neutron, it is also possible that the direction of **P** will change. If the frequency, Ω, with which the magnetic field changes is such that

$$\Omega = \mathrm{d}(\mathbf{B}/|\mathbf{B}|)/\,\mathrm{d}t \ll \omega_L, \qquad (4.4.2.19)$$

then the polarization vector follows the field rotation adiabatically. Alternatively, when $\Omega \gg \omega_L$, the magnetic field changes so rapidly that **P** cannot follow, and the condition is known as non-adiabatic fast passage. All spin-orientation devices are based on these concepts.

4.4.2.7.1. *Maintaining the direction of polarization*

A polarized beam will tend to become depolarized during passage through a region of zero field, since the field direction is ill defined over the beam cross section. Thus, in order to keep the polarization direction aligned along a defined quantization axis, special precautions must be taken.

The simplest way of maintaining the polarization of neutrons is to use a guide field to produce a well defined field **B** over the whole flight path of the beam. If the field changes direction, it has to fulfil the adiabatic condition $\Omega \ll \omega_L$, *i.e.* the field changes must take place over a time interval that is long compared with the Larmor period. In this case, the polarization follows the field direction adiabatically with an angle of deviation $\Delta\theta \leq 2\arctan(\Omega/\omega_L)$ (Schärpf, 1980).

Alternatively, some instruments (*e.g.* zero-field spin-echo spectrometers and polarimeters) use polarized neutron beams in regions of zero field. The spin orientation remains constant in a zero-field region, but the passage of the neutron beam into and out of the zero-field region must be well controlled. In order to provide a well defined region of transition from a guide-field region to a zero-field region, a non-adiabatic fast passage through the windings of a rectangular input solenoid can be used, either with a toroidal closure of the outside field or with a μ-metal closure frame. The latter serves as a mirror for the coil ends, with the effect of producing the field homogeneity of a long coil but avoiding the field divergence at the end of the coil.

4.4.2.7.2. *Rotation of the polarization direction*

The polarization direction can be changed by the adiabatic change of the guide-field direction so that the direction of the polarization follows it. Such a rotation is performed by a spin turner or spin rotator (Schärpf & Capellmann, 1993; Williams, 1988).

Alternatively, the direction of polarization can be rotated relative to the guide field by using the property of precession described above. If a polarized beam enters a region where the field is inclined to the polarization axis, then the polarization vector **P** will precess about the new field direction. The precession angle will depend on the magnitude of the field and the time spent in the field region. By adjustment of these two parameters together with the field direction, a defined, though wavelength-dependent, rotation of **P** can be achieved. A simple device uses the non-adiabatic fast passage through the windings of two rectangular solenoids, wound orthogonally one on top of the other. In this way, the direction of the precession field axis is determined by the ratio of the currents in the two coils, and the sizes of the fields determine the angle φ of the precession. The orientation of the polarization vector can therefore be defined in any direction.

In order to produce a continuous rotation of the polarization, *i.e.* a well defined precession, as required in neutron spin-echo (NSE) applications, precession coils are used. In the simplest case, these are long solenoids where the change of the field integral over the cross section can be corrected by Fresnel coils (Mezei, 1972). More recently, Zeyen & Rem (1996) have developed and implemented optimal field-shape (OFS) coils. The field in these coils follows a cosine squared shape that results from the optimization of the line integral homogeneity. The OFS coils can be wound over a very small diameter, thereby reducing stray fields drastically.

4.4.2.7.3. *Flipping of the polarization direction*

The term 'flipping' was originally applied to the situation where the beam polarization direction is reversed with respect to a guide field, *i.e.* it describes a transition of the polarization direction from parallel to antiparallel to the guide field and *vice versa*. A device that produces this 180° rotation is called a π flipper. A $\pi/2$ flipper, as the name suggests, produces a 90° rotation and is normally used to initiate precession by turning the polarization at 90° to the guide field.

The most direct wavelength-independent way of producing such a transition is again a non-adiabatic fast passage from the region of one field direction to the region of the other field direction. This can be realized by a current sheet like the Dabbs foil (Dabbs, Roberts & Bernstein, 1955), a Kjeller eight (Abrahams, Steinsvoll, Bongaarts & De Lange, 1962) or a cryoflipper (Forsyth, 1979).

Alternatively, a spin flip can be produced using a precession coil, as described above, in which the polarization direction makes a precession of just π about a direction orthogonal to the guide field direction (Mezei, 1972). Normally, two orthogonally wound coils are used, where the second, correction, coil serves to compensate the guide field in the interior of the precession coil. Such a flipper is wavelength dependent and can be easily tuned by varying the currents in the coils.

Another group of flippers uses the non-adiabatic transition through a well defined region of zero field. Examples of this type of flipper are the two-coil flipper of Drabkin, Zabidarov, Kasman & Okorokov (1969) and the line-shape flipper of Korneev & Kudriashov (1981).

Historically, the first flippers used were radio-frequency coils set in a homogeneous magnetic field. These devices are wavelength dependent, but may be rendered wavelength independent by replacing the homogeneous magnetic field with a gradient field (Egorov, Lobashov, Nazarento, Porsev & Serebrov, 1974).

In some devices, the flipping action can be combined with another selection function. The wavelength-dependent magnetic wiggler flipper proposed by Agamalyan, Drabkin & Sbitnev (1988) in combination with a polarizer can be used as a polarizing monochromator (Majkrzak & Shirane, 1982). Badurek & Rauch (1978) have used flippers as choppers to pulse a polarized beam.

In neutron resonance spin echo (NRSE) (Gähler & Golub, 1987), the precession coil of the conventional spin-echo configuration is replaced by two resonance spin flippers separated by a large zero-field region. The radio-frequency field of amplitude B_1 is arranged orthogonal to the DC field, B_0, with a frequency $\omega = \omega_L$, and an amplitude defined by the relation $\omega_1 \tau = \pi$, where τ is the flight time in the flipper coil and $\omega_1 = \gamma B_1$. In this configuration, the neutron spin precesses through an angle π about the resonance field in each coil and leaves the coil with a phase angle φ. The total phase angle after passing through both coils, $\varphi = 2\omega L/v$, depends on the velocity v of the neutron and the separation L between the two coils. Thus, compared with conventional NSE, where the phase angle comes from the precession of the neutron spin in a strong magnetic field compared with a static flipper field, in NRSE the neutron spin does not precess, but the flipper field rotates. Effectively, the NRSE phase angle φ is a factor of two larger than the NSE phase angle for the same DC field B_0. Furthermore, the resolution is determined by the precision of the RF frequencies and the zero-field flight path L rather than the homogeneity of the line integral of the field in the NSE precession coil.

4.4.2.8. *Mechanical choppers and selectors*

Thermal neutrons have relatively low velocities (a 4 Å neutron has a reciprocal velocity of approximately $1000\,\mu s\,m^{-1}$), so that mechanical selection devices and simple flight-time measurements can be used to make accurate neutron energy determinations.

Disc choppers rotating at speeds up to 20 000 revolutions per minute about an axis that is parallel to the neutron beam are used to produce a well defined pulse of neutrons. The discs are made from absorbing material (at least where the beam passes) and comprise one or more neutron-transparent apertures or slits. For polarized neutrons, these transparent slits should not be metallic, as the eddy currents in the metal moving in even a weak guide field will strongly depolarize the beam. The pulse frequency is determined by the number of apertures and the rotation frequency, while the duty cycle is given by the ratio of open time to closed time in one rotation. Two such choppers rotating in phase can be used to monochromate and pulse a beam simultaneously (Egelstaff, Cocking & Alexander, 1961). In practice, more than two choppers are generally used to avoid frame overlap of the incident and scattered beams. The time resolution of disc choppers (and hence the energy resolution of the instrument) is determined by the beam size, the aperture size and the rotation speed. For a realistic beam size, the rotation speed limits the resolution. Therefore, in modern instruments, it is normal to replace a single chopper with two counter-rotating choppers (Hautecler *et al.*, 1985; Copley, 1991). The low duty cycle of a simple disc chopper can be improved by replacing the single slit with a series of slits either in a regular sequence (Fourier chopper) (Colwell, Miller & Whittemore, 1968; Hiismäki, 1997) or a pseudostatistical sequence (pseudostatistical chopper) (Hossfeld, Amadori & Scherm, 1970), with duty cycles of 50 and 30%, respectively.

The Fermi chopper is an alternative form of neutron chopper that simultaneously pulses and monochromates the incoming beam. It consists of a slit package, essentially a collimator, rotating about an axis that is perpendicular to the beam direction (Turchin, 1965). For optimum transmission at the required wavelength, the slits are usually curved to provide a straight collimator in the neutron frame of reference. The curvature also eliminates the 'reverse burst', *i.e.* a pulse of neutrons that passes when the chopper has rotated by 180°.

A Fermi chopper with straight slits in combination with a monochromator assembly of wide horizontal divergence can be used to time focus a polychromatic beam, thus maintaining the energy resolution while improving the intensity (Blanc, 1983).

Velocity selectors are used when a continuous beam is required with coarse energy resolution. They exist in either multiple disc configurations or helical channels rotating about an axis parallel to the beam direction (Dash & Sommers, 1953). Modern helical channel selectors are made up of lightweight absorbing blades slotted into helical grooves on the rotation axis (Wagner, Friedrich & Wille, 1992). At higher energies where no suitable absorbing material is available, highly scattering polymers [poly(methyl methacrylate)] can be used for the blades, although in this case adequate shielding must be provided. The neutron wavelength is determined by the rotation speed, and resolutions, $\Delta\lambda/\lambda$, ranging from 5% to practically 100% ($\lambda/2$ filter) can be achieved. The resolution is fixed by the geometry of the device, but can be slightly improved by tilting the rotation axis or relaxed by rotating in the reverse direction for shorter wavelengths. Transmissions of up to 94% are typical.

4.4.3. Resolution functions (By R. Pynn and J. M. Rowe)

In a *Gedanken* neutron scattering experiment, neutrons of wavevector $\mathbf{k}_I$ impinge on a sample and the wavevector, $\mathbf{k}_F$, of the scattered neutrons is determined. A number of different types of spectrometer are used to achieve this goal (*cf.* Pynn, 1984). In each case, finite instrumental resolution is a result of uncertainties in the definition of $\mathbf{k}_I$ and $\mathbf{k}_F$. Propagation directions for neutrons are generally defined by Soller collimators for which the transmission as a function of divergence angle generally has a triangular shape. Neutron monochromatization may be achieved either by Bragg reflection from a (usually) mosaic crystal or by a time-of-flight method. In the former case, the mosaic leads to a spread of $|k_I|$ while, in the latter, pulse length and uncertainty in the lengths of flight paths (including sample size and detector thickness) produce a similar effect. Calculations of instrumental resolution are generally lengthy and lack of space prohibits their detailed presentation here. In the following paragraphs, the concepts involved are indicated and references to original articles are provided.

In resolution calculations for neutron spectrometers, it is usually assumed that the uncertainty of the neutron wavevector does not vary spatially across the neutron beam, although this reasoning may not apply to the case of small samples and compact spectrometers. To calculate the resolution of the spectrometer in the large-beam approximation, one writes the measured intensity I as

references